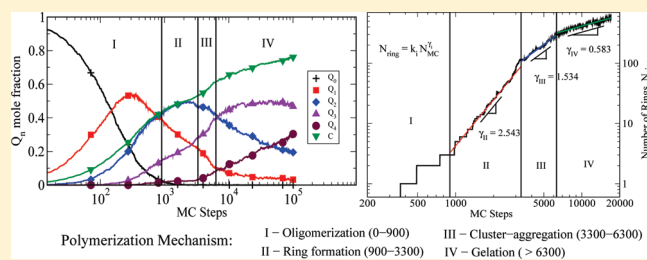


# Monte Carlo Simulations of Silica Polymerization and Network Formation

Ateeque Malani,<sup>†</sup> Scott M. Auerbach,<sup>\*,‡</sup> and Peter A. Monson<sup>\*,†</sup><sup>†</sup>Department of Chemical Engineering, University of Massachusetts, Amherst 01003, MA, United States<sup>‡</sup>Department of Chemistry and Chemical Engineering, University of Massachusetts, Amherst 01003, MA, United States

**ABSTRACT:** We present a new model and method for the Monte Carlo simulation of silica polymerization in aqueous solution. We focus on the idea that silica structures are built from corner sharing tetrahedra and these tetrahedra are the basic units of the model. Rather than use a reactive force field, the assembly of tetrahedral units is accomplished via Monte Carlo simulation in the reaction ensemble. The simplicity of the model and the use of the reaction ensemble make it possible to study silica polymerization for quite large system sizes, reaching a high degree of condensation under ambient conditions. We find that the reaction ensemble Monte Carlo simulation protocol can provide a description of the overall polymerization kinetics, after making some key assumptions. Very good agreement is obtained when comparing simulated and experimental evolutions of the  $Q_n$  distribution as a function of both time and degree of condensation, indicating an approximately linear relationship between physical time and number of Monte Carlo steps up to about 5 h. Analyses of cluster-size and ring-size distributions reveal that polymerization proceeds in the following main stages: oligomerization forming small units (0–1 h), ring formation (1–2.6 h), cluster aggregation (2.6–5.6 h), and finally cross-linking of the aging gel at later times.



Understanding the polymerization of silicic acid in aqueous solution has been an active area of research for some time.<sup>1,2</sup> This reaction system lies at the heart of sol–gel processing as well as the synthesis of porous materials such as zeolites<sup>3</sup> and ordered mesoporous materials.<sup>4,5</sup> Improved understanding of the fundamental mechanisms involved can be expected to have a significant impact in the control of material structure and properties in these systems. Silica polymerization has been studied both by experimental<sup>1,2,6–10</sup> and theoretical methods,<sup>11–15</sup> and significant progress has been made. Nevertheless, a complete understanding of the structural evolution of the system under different conditions remains elusive. Molecular modeling and simulation based on statistical mechanics have the potential for significant impact, and we will briefly review some of these developments below.<sup>16</sup> However, viewed from the perspective of statistical mechanics, silica polymerization is a very complex problem. The energy landscape of silica structures, as revealed by density functional theory (DFT) calculations of their binding energies,<sup>17,18</sup> suggests a multiplicity of nearly degenerate minima representing both crystalline and amorphous states separated by large barriers that depend on the connectivity of the polymerized silica in these structures. Metastability is ubiquitous, and the search for true equilibrium may be irrelevant to the problem of structural evolution of porous silica materials. In this paper, we report on simulation methods that shed light on silica polymerization pathways, which are of central importance to structure formation in silica materials.

Our own interest in this problem derives from work on understanding the synthesis of porous silica materials. We are interested in both the formation of all-silica zeolite frameworks, such as MFI (silicalite-1),<sup>19</sup> and ordered mesoporous silica materials.<sup>4,5,20</sup> In the first of these materials, the network structure is crystalline with the nanoscale order created by small structure directing agents or templates. In the second group of materials, the network structure is amorphous (similar to the structure of glass) with templating produced by larger surfactant molecules or block copolymers or both.<sup>4,5,20</sup> These types of materials represent two paradigms for the controlled synthesis of ordered nanoporous materials. We seek to understand both kinds of systems within a single nanoscale modeling framework. Essential to progress in this modeling program is a good method for describing silica polymerization under experimentally relevant conditions.

The initial targets for our modeling work are the experiments of Devreux et al.<sup>8,9</sup> on the polymerization of silicic acid under isoelectric (pH 2.5) conditions. These authors used NMR to study the kinetics of silica polymerization following hydrolysis of a silica source in aqueous solution. Of the three different silica sources used—tetraethoxysilane (TEOS), methyltriethoxysilane (MTEOS), and vinyltriethoxysilane (VTEOS)—we focus primarily on the results for TEOS, since

Received: March 8, 2011

Revised: July 1, 2011

Published: July 07, 2011

this leads to gelation at long times. Polymerization progress was tracked by measuring the  $Q_n$  distribution, where  $Q_n$  refers to a silicon atom connected to  $n$  bridging oxygen atoms, so that  $Q_0$  denotes silicic acid and  $Q_4$  denotes a silicon atom bonded to four bridging oxygens. The degree of condensation,  $c$ , where  $0 \leq c \leq 1$ , is then given by  $c = (1/f) \sum_{n=0}^f n q_n$ , where  $q_n$  is the mole fraction of  $Q_n$  silicon atoms and  $f$  is the coordination number of the network (normally  $f = 4$  for silica). ( $Q_n$  labels a silicon species, while  $q_n$  is the mole fraction of such a species.) Devreux et al.<sup>8</sup> identified three stages in the polymerization process: first the formation of oligomers of silicic acid, second the growth of fractal aggregates from these oligomers, and finally gelation through agglomeration of the fractal aggregates. We show below that our results are in excellent agreement with those of Devreux et al. but that they also reveal an important new growth stage at intermediate times focused on silica ring formation.

The earliest efforts to model silicic acid polymerization focused on solving the material balances for the various species involved together with reaction rate expressions.<sup>21–24</sup> Important input parameters for such approaches are the rate constants of the chemical reactions considered. Each silicon atom with coordination number 4 can be bound to three functional groups (Si–OR, Si–OH, and Si–OSi), resulting in 15 distinguishable silicon environments. At this level of speciation, 165 rate constants are required and it is difficult to estimate these from experiments.<sup>22</sup> In order to simplify the task, the rate constants were assumed to depend on functional groups alone, and were obtained from initial concentrations.<sup>21,22</sup> This level of modeling was able to predict reasonably the initial behavior of  $Q_0$ ,  $Q_1$ , and  $Q_2$ .<sup>25</sup> However, deviations from experimental behavior were observed at longer times.<sup>25</sup> Recently, these equations were solved using Monte Carlo simulations and it was shown that knowledge of nearest neighbor coordination and explicit cyclization needs to be incorporated to reproduce the experimentally observed  $Q_n$  distributions.<sup>26–28</sup> While this approach successfully predicts the evolution of the  $Q_n$  distribution for all  $n$ , it fails to reveal the spatial structures of the polymerized silica. Knowledge of this is necessary to understand and tailor the synthesis of templated nanoporous silica materials. Approaches based on atomic-level models are thus necessary for moving this field forward.

The major challenges for modeling silicic acid polymerization using molecular simulations are handling large system sizes, accessing long time scales, and developing suitable atomistic interaction potentials. The need for large system sizes arises from the dilute concentration of aqueous silicic acid studied in characterization experiments such as NMR.<sup>8,9</sup> Long times are required to complete the polymerization process under experimentally relevant conditions, for example,  $\sim 200$  days for 85% conversion of silicic acid to silica with an initial concentration of  $1\text{Si}(\text{OH})_4:6\text{H}_2\text{O}:10\text{C}_2\text{H}_5\text{OH}$  at room temperature and pH 2.5.<sup>8</sup>

Despite these challenges, there have been encouraging efforts to study polymerization using atomistic simulations.<sup>11–16,29–31</sup> Feuston and Garofalini developed a detailed atomistic force-field that describes condensation and hydrolysis reaction events.<sup>11</sup> Molecular dynamics (MD) using such potentials illustrates that monomer–monomer and monomer–dimer condensation reactions are of the  $\text{S}_{\text{N}}2$  type.<sup>11</sup> In such simulations, the accessible time scale is on the order of nanoseconds, which limits the ability to generate substantial polymerization. In

order to achieve a high degree of condensation within accessible simulation time scales, the rates of reactive events were increased by increasing both the concentration and temperature to very high values relative to those in the experimental studies. This enabled the study of silica gel formation within reasonable MD time scales, as shown in several studies of this type.<sup>12–15</sup> Some of the characteristics of the simulated polymerized silica such as ring-size distribution, fractal dimension, and bond lengths agree with experimental observations.<sup>12,14,15</sup> However, due to the elevated temperature and concentration used, the time evolutions of the  $Q_n$  distribution obtained from these simulations do not agree with experimental results.<sup>12–14</sup> With the current computational resources and available potential models for the water and silica components, analyzing much larger systems for much longer times under experimental conditions is not feasible.

It is also worthwhile to mention complementary studies of silica dissolution, a problem that has been studied for decades using both experiments<sup>32–34</sup> and computational models.<sup>35–37</sup> We note in particular recent work by Nangia and Garrison<sup>37</sup> in which they simulated silica dissolution using reaction ensemble and configurational bias Monte Carlo techniques.<sup>37</sup> This study suggests that a stepwise dissolution mechanism ( $Q_i \rightleftharpoons Q_{i-1}$ ) is more realistic than a direct (one-step) dissolution process ( $Q_i \rightleftharpoons Q_0$ ). While the methodology of Nangia and Garrison is able to efficiently sample the reaction events, the level of detail in their atomistic model limited their study to smaller system sizes with high concentrations of silica.<sup>37</sup>

In this paper, we describe a new approach for modeling silica polymerization based on a somewhat different physical perspective. We note that polymerized silica structures in nature are typically built from corner sharing tetrahedra, prompting us to make such tetrahedra the basic units of our model. Rather than use a reactive force field, the assembly of tetrahedral units is accomplished via Monte Carlo simulation in the reaction ensemble. The simplicity of the model and the use of the reaction ensemble make it possible to study silica polymerization for quite large system sizes, reaching a high degree of condensation under ambient conditions, although we lose some information on the dynamics of individual reactive events. The reaction ensemble Monte Carlo simulation protocol is designed so that the evolution of states to some extent captures the real mechanism. This requires making key assumptions described in detail below. We find that the approach yields an evolution of the  $Q_n$  distribution with both time and the degree of condensation that agrees well with experiment, indicating an approximately linear relationship between physical time and number of Monte Carlo steps. In addition, the calculations reveal the structure of the polymerized silica and insights into the polymerization mechanism. A preliminary report of this work was presented elsewhere;<sup>38</sup> here, we give a more detailed presentation of the methods with additional results and discussion.

The remainder of this paper is organized as follows: In section 1, we discuss the model and the simulation strategy together with details of the Monte Carlo simulations performed. In section 2, we report our results on the  $Q_n$  distribution, the mechanism of polymerization, and the structure of the polymerized silica. In section 3, we offer a summary of our findings and some concluding remarks. The Appendix outlines the simulation algorithm in detail.

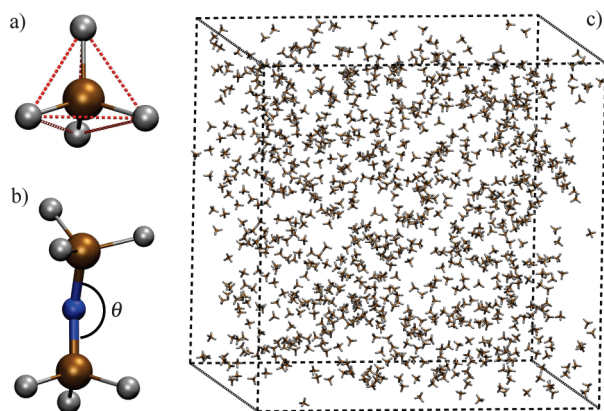


**Figure 1.** (a) Tetrahedral structure of silicic acid ( $\text{Si}(\text{OH})_4$ ) represented by the hard core silicon atom (brown) in the center and four hydroxyl groups (gray) at the periphery. The (red) dashed lines connecting the hydroxyl groups indicate the springs between them. (b) The dimer formed after the condensation of two silicic acid forming a bridging oxygen (blue) with an Si–O–Si angle of  $\theta$ . (c) The monomeric system before reaction in the cubic box of 104 Å consisting of 1000  $\text{Si}(\text{OH})_4$  molecules.

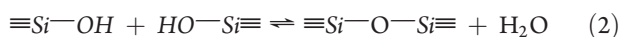
## 1. MODEL AND SIMULATION METHODOLOGY

**1.1. Molecular Model.** Our approach is based on an idea presented by Astala et al.<sup>18</sup> for modeling the mechanical properties of crystalline silica solids. In that model, silica is treated as collections of flexible, corner-sharing tetrahedra. We generalize this to model silica polymerization by considering a  $Q_n$  silica unit ( $\text{Si}(\text{OH})_{4-n}\text{O}_n$ ) as a tetrahedron with a hard sphere in its center and four point particles representing hydroxyl groups (OH) and/or bridging oxygens (BO) in the periphery, as shown in Figure 1a. Following Wu and Deem,<sup>39</sup> we make no explicit distinction between OH and BO groups. Flexible tetrahedra are maintained via harmonic springs between BO and/or OH groups according to

$$U_1 = \sum_{i=1}^3 \sum_{j=i+1}^4 \frac{k_S}{2} (|\mathbf{r}_i - \mathbf{r}_j| - r_0)^2 \quad (1)$$

where  $U_1$  is the potential energy due to distortion of a single tetrahedron,  $\mathbf{r}_i$  is the three-dimensional position of the  $i$ th BO/OH vertex,  $k_S$  is the spring constant, and  $r_0$  is the equilibrium distance between two such vertices. The value of  $r_0$  is set at 2.61 Å<sup>18</sup> based on the geometry of the silica tetrahedron (Si–O bond length = 1.6 and O–Si–O angle = 109.47°<sup>3</sup>). The Si hard sphere potential prevents unphysical interpenetration of the tetrahedra, with the hard sphere diameter set at  $\sigma_{\text{Si-Si}} = 2$  Å, chosen so that all possible overlapping conformations between two hydroxyl groups are allowed. One could choose smaller values of  $\sigma_{\text{Si-Si}}$ ; however, that would only serve to increase computational cost.

For silicic acid polymerization, a general condensation/hydrolysis reaction can be written as



where the forward reaction is condensation and the backward one is hydrolysis. One can view the polymerization process as the assembly of  $\text{Si}(\text{OH})_4$  tetrahedra via condensation reactions, forming a complex network with stoichiometry  $\text{Si}_x\text{O}_y\text{H}_z$  where  $y/x \rightarrow 2$  and  $z/x \rightarrow 0$ . After a condensation reaction, two tetrahedra are joined via a bridging oxygen (Si–O–Si), as shown

**Table 1. Parameters of the Flexible Tetrahedron Model**

$\sigma_{\text{Si-Si}}$ (Å)	2
$k_S$ ( $\text{kJ mol}^{-1} \text{Å}^{-2}$ )	851
$k_A$ ( $\text{kJ mol}^{-1}$ )	226.74
$r_0$ (Å)	2.61
$\theta_0$ (deg)	155

in Figure 1b. In the resulting network, the Si–O–Si angles formed by the bridging oxygens are restricted using a harmonic potential:

$$U_2 = \frac{k_A}{2} (\cos \theta - \cos \theta_0)^2 \quad (3)$$

where  $\theta$  is the Si–O–Si angle formed by the bridging oxygen,  $\theta_0$  is a reference angle, and  $k_A$  is the force constant. The force constants,  $k_S$  and  $k_A$ , together with  $\theta_0$  were taken from the work of Astala et al.,<sup>18</sup> where they were fitted to DFT calculations of bulk moduli of various silica polymorphs. The parameter values are given in Table 1. We note that the reference Si–O–Si angle of 155° falls roughly midway in the range of observed Si–O–Si angles in silica materials: 130–180°. This angle was determined by optimizing infinite silica chains using periodic DFT,<sup>40</sup> hence avoiding the perturbing effects of hydrogen bonding in small clusters, and network effects in three-dimensional solids. The angular force constant is small enough to allow a range of Si–O–Si angles, while being large enough to reproduce bulk moduli of (relatively incompressible) silica polymorphs. These are the only potential functions considered in our model. The change of electronic energy during condensation/hydrolysis reactions is included in the standard Gibbs free energy of reaction, as described below.

**1.2. Monte Carlo Simulations.** The sampling of reaction events in our simulations of silica polymerization is accomplished by using the reaction ensemble Monte Carlo (REMC) method.<sup>41,42</sup> The REMC method eliminates the need for reactive force fields to bring about assembly of the polymerized silica network. The price for this is that we cannot describe the kinetics of individual condensation/hydrolysis events. Using REMC makes it feasible to study polymerization at ambient temperatures and at low silica concentrations, both of which have been a challenge for other atomistic simulation approaches.<sup>11–15</sup> We can also study quite large system sizes on a modest computation budget. Our choice for the REMC technique is further supported by the recent simulation study of Nangia and Garrison<sup>37</sup> where they studied silica dissolution using REMC techniques.

As we mentioned earlier, we are interested not just in capturing the structure of the polymerized state but also in modeling the pathways to silica polymerization. We must contrive to have our REMC simulations mimic these pathways. In the REMC method, the evolution of the system is determined by three key inputs: the standard Gibbs energy of reaction, the potential energies of silica distortion described above, and the probabilities of the different kinds of MC moves. In our simulations, the MC moves performed are displacement of BO or OH groups, displacement/rotation of  $\text{Si}(\text{OH})_{4-n}\text{O}_n$  tetrahedra, displacement of clusters, and condensation/hydrolysis moves. Attempted displacements of BO/OH groups, displacements of tetrahedra, and rotations of tetrahedra are accepted with the usual Metropolis probability determined by the Boltzmann factor,  $\exp(-\beta\Delta U)$ , where  $\beta = 1/k_B T$ ,  $T$  is the temperature,  $k_B$  is Boltzmann's constant, and  $\Delta U$  is the change in total potential

energy. By adjusting the relative attempt probabilities of these moves, we can tune the dynamics of the system in MC “time”. In the end, our goal is a Markov chain of states that closely resembles the actual silica polymerization process.

We now consider the translation moves for the various silica monomers and clusters in the system. In general, the diffusion of particles in a solvent is, broadly speaking, slowed by the drag force created by the solvent. We therefore adjust the probability of particle displacement based on cluster size in order to reflect solvent drag. The drag force exerted would change the translation mobility of a particle or cluster as quantified by the Stokes–Einstein equation:

$$D_{cl} = \frac{k_B T}{6\pi\eta r_{cl}} \quad (4)$$

where  $D_{cl}$  is the diffusivity of a cluster,  $\eta$  is the viscosity of the medium, and  $r_{cl}$  is the radius of a cluster. The cluster radius is related to cluster size,  $N_{cl}$ , according to  $r_{cl} \propto N_{cl}^\alpha$ , where  $\alpha$  is an exponent whose value depends on cluster shape. For example, in the case of a sphere we have  $\alpha = 1/3$ , while for rod-shaped particles  $\alpha = 1$ . The actual geometry and connectivity of clusters are continuously changing, and it is not practical to track this during the simulation, so we have used a fixed value of  $\alpha = 1$  for simplicity in our simulations. This simplification means that  $D_{cl} \propto 1/N_{cl}$ . On the basis of this scaling, the probability to move a cluster of size  $N_{cl}$ , relative to that for moving a monomer, is reduced in our algorithm by the factor  $1/N_{cl}$ .

Silicic acid polymerization involves a multicomponent system with many reactions. In the REMC method, the probability for reactive moves is given by

$$P_{rxn} = e^{-\beta\Delta U} V^{-\bar{\nu}} \prod_{i=1}^{n_c} \frac{N_i!}{(N_i + \nu_i)!} q_i^{\nu_i} \quad (5)$$

where  $\Delta U$  is the change in potential energy arising from tetrahedral and network distortions;  $V$  is the volume;  $n_c$  is the total number of components;  $\bar{\nu} = \sum_{i=1}^{n_c} \nu_i$ ; and  $q_i$ ,  $N_i$ , and  $\nu_i$  are the molecular partition function, number of molecules, and stoichiometric coefficient of component  $i$ . The molecular partition functions  $q_i$  are related to the equilibrium constant and standard Gibbs energy of reaction via  $K_{eq} = \exp[-\Delta G^0/k_B T] = \prod_{i=1}^{n_c} q_i^{\nu_i}$ . We simplify the calculations by using the standard Gibbs energy of reaction as an input parameter to the calculation. We further assume that this value is unchanged for all reaction types in the system. This eliminates the essentially impossible task of determining the free energies for the very large number of reactions that occur in the polymerization process. The approximation of constant reaction free energy is supported by DFT studies of the reaction energetics for species of various  $Q_n$ .<sup>43,44</sup> We have used  $K_{eq} = 500$  in this work and in our previous report,<sup>38</sup> corresponding to a condensation free energy of  $-3.7 \text{ kcal mol}^{-1}$ , which is in reasonable agreement with the electronic energy change of  $-3.2 \text{ kcal mol}^{-1}$  obtained from DFT for silicic acid dimerization in water.<sup>45</sup>

In our implementation of REMC, we use two methods to make trial condensation reactions, depending on whether the OH groups are in the same cluster or in different clusters (or monomers). When two randomly selected hydroxyl groups are part of different clusters and/or monomers, we translate the two selected monomers/clusters toward each other so that the two selected OH groups coincide at the midpoint on the line connecting the two OH groups. The two OH groups are then

replaced by a BO, completing the attempted move. Compared with an unbiased simulation where the OH groups come together via stochastic motion, our approach greatly increases the reaction rate. In order to make our MC trajectory more reflective of the actual mechanism, we reduce the acceptance probability by an estimate of the number of steps required to bring the two groups together via short-range diffusive moves. We make the assumption that this is proportional to the square of the intercluster distance (assuming diffusive motion) and inversely related to the diffusivity. As such, the effective number of MC steps required to bring together two clusters of size  $i$  and  $j$  is estimated as

$$N_{MC,ij} \propto \frac{|\mathbf{r}_{OH,i} - \mathbf{r}_{OH,j}|^2}{D_{cl,i} + D_{cl,j}} = k \frac{|\mathbf{r}_{OH,i} - \mathbf{r}_{OH,j}|^2}{1/N_{cl,i} + 1/N_{cl,j}} \quad (6)$$

where  $N_{MC,ij}$  is the number of MC moves required to displace two clusters  $i$  and  $j$  such that two hydroxyl groups overlap,  $\mathbf{r}_{OH,i}$  are the coordinates of the OH group on cluster  $i$ , and  $k$  is a proportionality constant. The value of the proportionality constant is estimated on the basis of a nonreacting silicic acid (monomeric) system. Before the condensation reaction is started, we assume that, for a system containing  $N$  monomers, the average distance that can be traversed by a monomer without collision is  $(V/N)^{1/3}$ , based on a random initial arrangement of monomers. The value of  $k$  is calculated using eq 6 based on the assumption that two monomers ( $i$  and  $j$ ,  $N_{cl,i} = 1 = N_{cl,j}$ ) can be displaced by a distance  $|\mathbf{r}_{OH,i} - \mathbf{r}_{OH,j}| = (V/N)^{1/3}$  in one MC move ( $N_{MC,ij} = 1$ ), which gives  $k = 2(N/V)^{2/3}$ . On the basis of these assumptions, we correct for translational bias by multiplying the reaction probability by the factor  $1/N_{MC,ij}$ .

We emphasize that eq 6 underestimates  $N_{MC,ij}$  because it assumes that two clusters diffuse on the line joining two hydroxyl groups (OH<sub>*i*</sub> and OH<sub>*j*</sub>), instead of treating the full three-dimensional stochastic motion. In three-dimensional motion of particles, there is a finite nonzero probability that they will never contact each other, which makes it impossible to estimate any mean contact time. This is one of the reasons, when reactions are performed in the usual way, i.e., reaction of two particles on collision, that leads to few reaction events and requires high density and temperature to increase probability of collision.<sup>12,13</sup> When MC simulations were performed with a similar approach, we observed only one successful condensation reaction during 1 million steps. In such a scenario, we used the above one-dimensional, directed-motion estimate as an initial guide to perform the simulations. As a consequence of underestimating  $N_{MC,ij}$ , we may expect regimes in which cluster aggregation is more likely in our simulations than in experiments. This is discussed below in the Results and Discussion section. Estimating better three-dimensional contact times ( $N_{MC,ij}$ ) is an important area for future development of our modeling approach.

For two randomly selected OH groups that are part of the same cluster, we represent the condensation reaction by replacing them with a bridging oxygen positioned at their center of mass. However, after such a reaction, the configuration of atoms around the condensing OH groups is severely distorted and should relax<sup>12</sup> to avoid a substantial energy penalty for the condensation reaction. We have found that we can improve the description of this reaction move by relaxing the system in the direction dictated by the forces on the cluster, i.e., by force–bias MC. After implementing the reaction move as described above, we carry out a sequence of 500 MC steps where in each step we

displace all vertices of a given cluster in the direction of force. The choice of 500 steps is somewhat arbitrary; it corresponds roughly to 50 ps of physical time assuming that standard thermal fluctuations of tetrahedral vertices lead to a diffusivity of  $10^{-5}$  cm<sup>2</sup>/s.<sup>38</sup> After 500 MC steps, the acceptance probability is calculated using eq 5, including the change in cluster energy due to cluster relaxation. This is the only move where cluster relaxation is incorporated. If the move were rejected by the Metropolis criterion, then the entire reaction move including the cluster relaxation would be rejected and the old configuration retained.

The directed motion during cluster relaxation (as opposed to random motion) imposes a bias into the system. This bias cannot be removed completely but can be mitigated by employing few such force–bias condensation moves. We only attempted such moves in 10% of all intracluster condensation moves. We found that about 5% of the total attempted force–bias intracluster condensation moves were accepted. We might expect to see an increase in bias due to force–bias moves with increasing system size because of stretching Si–O bonds over longer distances. However, we have observed that results for different system sizes are essentially the same. We studied systems containing 343, 432, 1000, and 2000 monomers, and observed no significant changes in evolution of the  $Q_n$  distribution. This suggests that the bias from force–bias moves is small, and does not appreciably affect the final system equilibrium. Complete descriptions of the condensation and force–bias moves are given in the Appendix.

The hydrolysis reaction is attempted by replacing a randomly selected bridging oxygen with two hydroxyl groups. Because the overlapping between hydroxyl groups is allowed in our model, both of the newly generated hydroxyl groups are placed at the location of the former bridging oxygen. Their positions equilibrate through subsequent MC displacements. After this, the change in potential energy (mainly due to removal of an Si–O–Si angle potential, eq 3) is calculated and the move is accepted with the REMC reaction probability (eq 5).

In addition to cluster translation, it might be assumed that a cluster rotation move could be used in the simulations. However, once a cluster spans the simulation cell, cluster rotation moves create huge distortions in some bond lengths because of periodic boundary conditions. Due to the large energy penalty that results from bond distortion, acceptance probabilities of such moves become extremely small. Because such large clusters form very early in silica polymerization (see section 2.1.3), we do not attempt cluster rotation in our simulations.

**1.3. Computational Details.** Each simulation was started from a random initial configuration of 1000 monomers in a cubic box under periodic boundary conditions with an edge length of 104 Å at 300 K (Figure 1c). This is a large system size compared with other simulation studies, in particular, where 216, 512, and 729 monomers were used by Garofailini et al.,<sup>12</sup> Bhattacharya et al.,<sup>14</sup> and Rao et al.,<sup>13</sup> respectively. The monomer density corresponds to the experimental conditions studied by Devreux et al.<sup>8</sup> The monomers were equilibrated for 0.1 million steps before attempting reaction moves. A MC step is defined as a set of  $N$  attempted moves where  $N$  is the system size (number of monomers = 1000). After the equilibration period, reactive moves were attempted, and the simulation was performed for another 0.1 million MC steps. The attempt probabilities for different trial MC moves are translation of Si(OH)<sub>4-n</sub>O<sub>n</sub> (0.34), rotation of Si(OH)<sub>4-n</sub>O<sub>n</sub> (0.34), displacement of BO/OH vertices (0.2), cluster displacement (0.1), and reaction moves

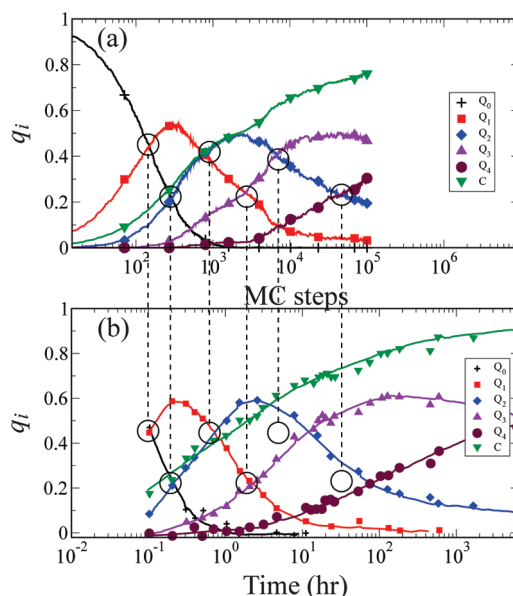


**Figure 2.** Evolution of  $Q_n$  distribution during polymerization obtained from simulations (a) and experiments (drawn by extracting data from Devreux et al.<sup>8</sup>) (b).

[condensation (0.01)/hydrolysis (0.01)]. The above attempt probabilities of various trial moves were determined on the basis of the following heuristic approach. (a) The motion of combined tetrahedral units is more important than individual atomic motions hence higher probabilities of the trial MC moves of tetrahedra units. (b) Due to low concentrations of monomers (5% mole), reaction events are much less probable. Changes in these attempt probabilities for the various moves would change the dynamics of the polymerization in MC “time”.

We analyzed structural descriptors to shed light on the polymerization process. These descriptors include distributions over bond lengths and angles, the total number of rings, the cluster-size distribution, the ring-size distribution, and the fractal dimension. There are numerous ways to define basic rings in the network structure, and in this case, we have used the primitive-ring definition to obtain ring-size distributions.<sup>46</sup> According to this definition, primitive rings are those that cannot be divided into two smaller rings. The cluster-size distribution was obtained using the method of Sevick et al.<sup>47</sup>

## 2. RESULTS AND DISCUSSION

**2.1. Mechanism of Polymerization.** Traditionally, the  $Q_n$  distribution is monitored in experiments as a probe of silica polymerization.<sup>1,8</sup> Figure 2a illustrates the variation in the concentration profile of the  $Q_n$  distribution as a function of the number of MC steps obtained from simulations. Also shown is the evolution of the degree of condensation,  $c$ . To compare the evolution of the  $Q_n$  distribution obtained from simulations with corresponding experimental data requires a mapping between MC steps and physical time. We establish the relationship between physical time and MC “time” by defining a common reference time using a point shared by the simulated and experimental  $Q_n$  distributions. In the experimental results, the first point is reported at 0.1 h at which the  $Q_0$  and  $Q_1$  profiles cross each other with mole fractions of  $q_0 = q_1 \cong 0.45$ . The corresponding situation in the MC simulation is observed at

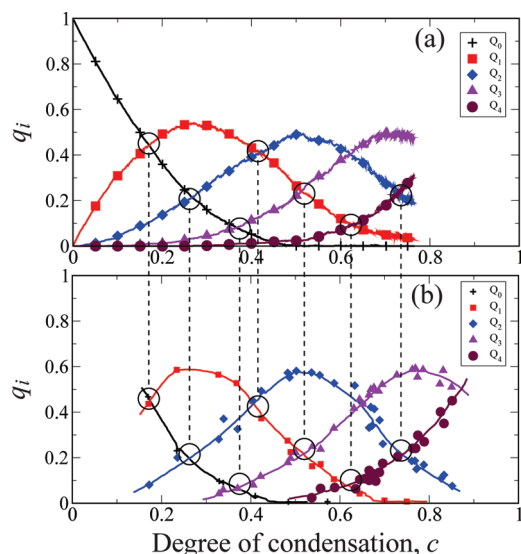


**Figure 3.** Variation of  $Q_n$  distribution as a function of degree of condensation obtained from simulations (a) and experiments (drawn by extracting data from Devreux et al.<sup>8</sup>) (b).

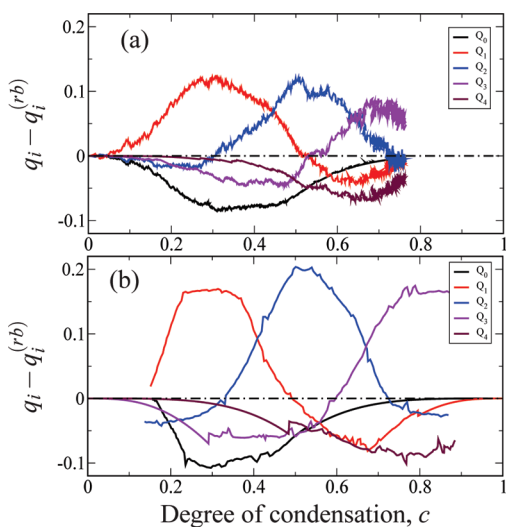


**Figure 4.** Difference of  $Q_n$  distribution obtained from the random branching model from simulations (a) and experiments (drawn by extracting data from Devreux et al.<sup>8</sup>) (b).

148 MC steps. We use this as the common reference point to compare simulation with experiment, as shown in Figure 2. If simulated and experimental  $Q_n$  distributions match beyond this single alignment point, it suggests that physical time is roughly proportional to the number of MC steps, and that our simulation has captured the key mechanistic aspects of silica polymerization.

Figure 2 shows that the simulation accurately captures the initial evolution of the  $Q_n$  distribution, with discrepancies emerging only at later times ( $\sim 5$  h). The mole fractions of  $Q_3$  and  $Q_4$  increase more rapidly in the simulations as compared with experiments. This discrepancy may be due to the one-dimensional approximation for the diffusive cluster contact time (i.e.,  $N_{MC,ij}$ ), which leads to faster cluster aggregation. Despite this discrepancy, the simulations capture much of the time dependence of

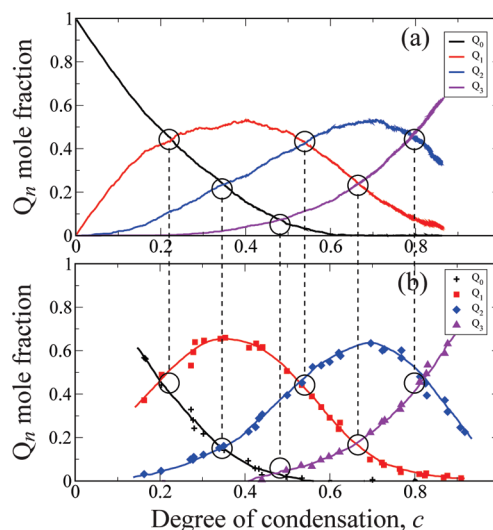


**Figure 5.** Variation of  $Q_n$  distribution as a function of degree of condensation for the  $\text{Si}(\text{OH})_3\text{OR}$  system obtained from simulations (a) and experiments (drawn by extracting data from Devreux et al.<sup>8</sup>) (b).

the  $Q_n$  distribution, including the progression of maxima in the  $q_n$  mole fractions and the values of these maxima.

Another way to compare the simulation with experiment is to plot the  $q_n$  mole fractions versus the degree of condensation  $c$ , which increases monotonically with time. In this way, we eliminate the issue of relating physical time with MC steps. The  $Q_n$  distributions vs degree of condensation from experiment and simulation are compared in Figure 3, which shows excellent quantitative agreement in all the crossing point locations and heights. We may thus be tempted to conclude that our simulations do indeed capture key aspects of the mechanism of silica condensation. However, before drawing such a conclusion, we now apply a stricter test of agreement between experiment and simulation.

One interesting feature of the experimental results<sup>8</sup> is the quite close agreement between the  $Q_n$  distribution versus  $c$  and that from a random branching model which gives<sup>8</sup>

$$q_n^{(rb)} = \frac{f!}{n!(f-n)!} c^n (1-c)^{f-n} \quad (7)$$

A more stringent test of our results is to replot the  $Q_n$  distributions versus  $c$  expressed as a deviation from the random branching model. By focusing on deviations, the graph scaling reveals more detailed structure, as shown in Figure 4. We see that simulation and experimental results depart from the random branching model in quite similar ways, indicating that the simulations capture the underlying statistics of branching. We infer from this fact that the simulations also capture important aspects of the branching mechanism. Indeed, a change in mechanism would change the evolution of  $Q_n$  distributions as a function of the degree of condensation.<sup>8</sup> For example, if the reaction mechanism were to favor formation of linear chains, then the reaction would stop at  $c = 0.5$  and the system would form one or more linear chains consisting mostly of  $Q_2$  silicons.

By making one of the vertices nonreactive in each model, we can study the polymerization process starting from MTEOS or VTEOS as the silica source, where the coordination number ( $f$ ) around each tetrahedron falls to 3. Results for the evolution of

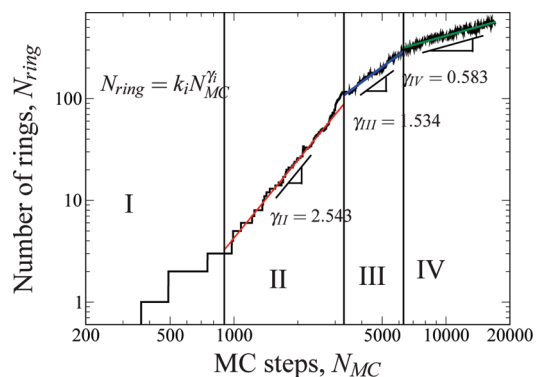


**Figure 6.** Evolution of the number of rings during MC simulation. The graph indicates four regimes distinguished by different power-law exponents ( $\gamma$ ) controlling rates of ring formation: (I) oligomerization (0–900 MC steps), (II) ring formation (900–3300 MC steps,  $\gamma_{II} = 2.5$ ), (III) cluster-aggregation (3300–6300 MC steps,  $\gamma_{III} = 1.5$ ), and (IV) gel aging ( $\geq 6300$  MC steps,  $\gamma_{IV} = 0.6$ ).

the  $Q_n$  distribution with  $c$  are shown in Figure 5. Again, we see that the agreement is very good. There is no  $Q_4$  silica in the system due to only three hydrolyzable groups on the silica source. The results expressed as a departure from the random branching model (data not shown) give a similar quality of agreement with experiment as those in Figure 4.

Despite the lack of an MC simulation clock (as exists in typical kinetic MC of reaction systems) and the simplicity of the model, the simulation results for the evolution of the  $Q_n$  distribution are in remarkable agreement with experiment. This agreement suggests that silica polymerization kinetics are not limited by individual reaction events and their barriers but rather by network structural constraints, which are included in our model via the potential energy changes associated with distorting the corner sharing tetrahedra and their spatial configuration (via the Si–O–Si bond angles). This is a fascinating result in that the mechanism of a reaction system is dominated by condensed phase interactions. This insight opens the door to future modeling work showing how network distortions determine time scales of reactive events in silica polymerization.

The evolution of the  $Q_n$  distribution alone does not elucidate the different stages of silica polymerization. To shed light on this, we have studied three structural descriptors: the total number of rings in the system, the cluster-size distribution, and the ring-size distribution. By analyzing these, we have found that silica polymerization proceeds in four stages: oligomerization (0–900 MC steps), ring formation (900–3300 MC steps), cluster aggregation (3300–6300 MC steps), and gel aging (6300–100 000 MC steps). The transition between each stage is signaled by a change in the scaling behavior of the rate of ring formation (Figure 6, *vide infra*), and by changes in the evolution of the cluster-size and ring-size distributions. We now discuss each stage in detail, beginning with oligomerization.

**2.1.1. Oligomerization (0–900 MC Steps).** In our simulation of silica polymerization, dimerization occurs in few MC steps, decreasing the monomer concentration ( $q_0$ ) as shown in Figure 2a. In the experiments at 6 min from the start of reaction, the  $Q_0$  and  $Q_1$  silica species attain mole fractions of 0.45, indicating a relatively rapid dimerization reaction<sup>8</sup> (Figure 2b). Dimerization proceeds with the further formation of oligomers, with the oligomers formed both by monomer–dimer

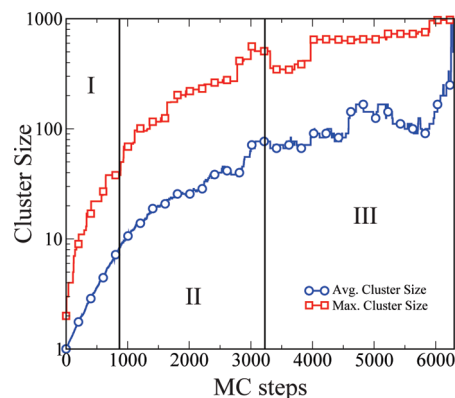


**Figure 7.** Evolution of the average and maximum cluster sizes observed during the MC simulation. The profile indicates three distinct regions where the behavior of the cluster size changes. These regions I–III correspond to oligomerization, ring formation, and cluster aggregation stages of polymerization, respectively.

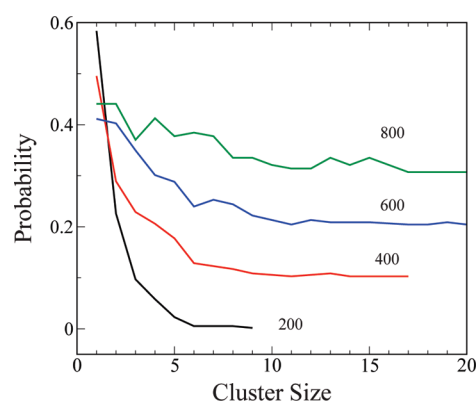


**Figure 8.** Evolution of the cluster-size distribution during the oligomerization stage corresponding to various MC steps in simulations. For clarity, the curves are displaced 0.1 units along the y-axis.

(or oligomer) as well as dimer–dimer (or oligomer–oligomer) reactions. The rapid oligomerization is due to the high concentration of hydroxyl groups leading to high collision probability, which in turn is also favored by the high monomer diffusivity compared to the diffusivity of larger oligomers. Polymerization can proceed via two reactions, cluster–cluster aggregation or cross-linking condensation reactions. At this early stage, the high mobility of clusters due to smaller size minimizes diffusion limitations for cluster–cluster aggregation reactions. In addition, the low concentration of large clusters limits ring formation, and we see a negligible number of rings in this regime. Thus, this regime is dominated by the aggregation of monomers and small oligomers. This observation is consistent with previous mathematical modeling approaches that capture the initial  $Q_n$  distribution, where diffusion limitation was ignored and polymerization was modeled on the basis of rate equations of different species.<sup>21,22</sup>

The concentrations of oligomers cannot be inferred from the  $Q_1$  and  $Q_2$  concentrations alone, necessitating the determination of the average and maximum cluster sizes during the simulation, shown in Figure 7. During this regime, the average cluster size increases to about eight tetrahedra. Figure 8 shows normalized

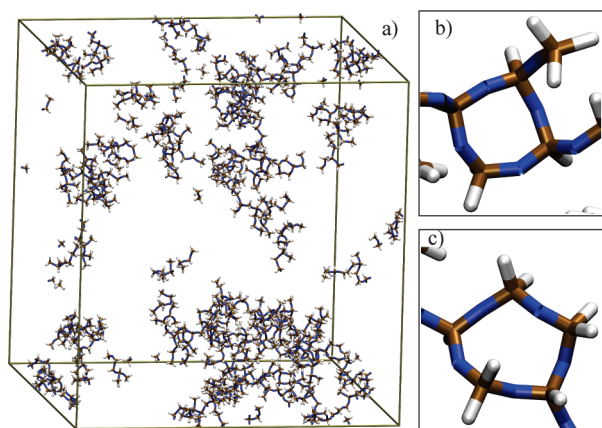


**Figure 9.** (a) The oligomers with rings, formed during the ring-formation stage. The brown, blue, and gray spheres indicate silicon, bridging oxygen, and hydroxyl groups, respectively. The snapshot exhibits concentration inhomogeneity and cluster-size distribution observed at 2000 MC steps during polymerization. Subfigures b and c are examples of four- and five-membered rings observed in this snapshot.

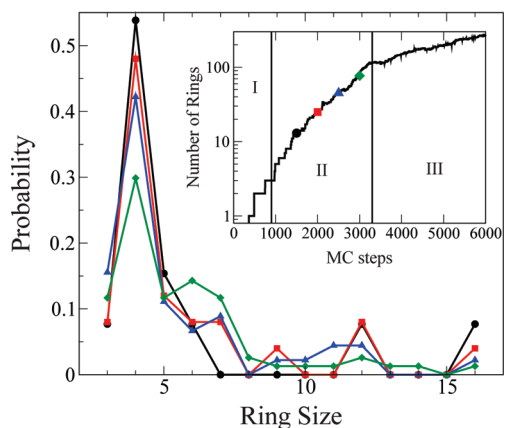


**Figure 10.** Evolution of the ring-size distribution during the ring-formation stage corresponding to different MC steps (1500 (○), 2000 (□), 2500 (△), and 3000 (◇)). The inset indicates the variation of the number of rings during the MC simulations.

cluster-size distributions at various times during the oligomerization stage. The distributions are displaced by 0.1 units along the y-axis for clarity. It is observed that, in the initial stages of polymerization, oligomers of small units are formed, ranging in size from 1 to 40 monomers, as shown in Figures 7 and 8. The degree of condensation reaches 0.43 during this stage (0–900 MC steps), suggesting that the oligomerization regime corresponds to the first hour of experiment, based on our earlier comparison in Figure 2. The reaction can proceed either by cluster–cluster aggregation or by cross-linking within the oligomers to form the rings. If the reaction were to proceed via cluster–cluster aggregation, then the cluster-size distribution should move rapidly toward larger cluster sizes, which is not observed in our simulations (Figure 7). This indicates that further reaction proceeds instead by ring formation, which we now discuss.

**2.1.2. Ring Formation (900–3300 MC Steps).** If polymerization were to continue via cluster–cluster aggregation (as the case

**Table 2.** Cluster-Size Distribution for Various MC Steps during the Cluster–Cluster Aggregation Regime (3300–6300 MC Steps)<sup>a</sup>

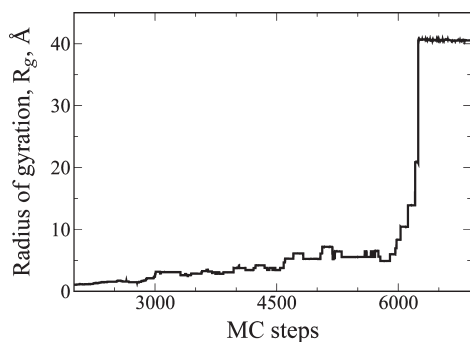
3400		4300		5300		6300	
<i>n</i>	<i>N</i> ( <i>n</i> )						
2	1	1	1	1	2	1000	1
9	1	2	1	2	1		
11	1	4	1	7	1		
12	1	12	1	22	1		
13	1	13	1	30	1		
30	2	21	1	207	1		
33	2	31	1	730	1		
41	1	53	1				
53	1	212	1				
91	1	651	1				
147	1						
151	1						
344	1						

<sup>a</sup>*N*(*n*) is the number of clusters of size *n* observed.

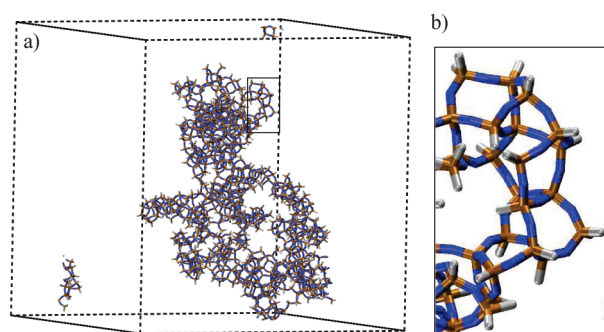
in oligomerization), then the concentration of both linear and branched polymers would continue to grow. However, when the mole fractions  $q_1$ ,  $q_2$ , and  $q_3$  are analyzed in detail in the range of 900–3300 MC steps, we observe a decrease in  $q_1$  and an increase in  $q_2$  and  $q_3$  (Figure 2a). This indicates changes in the network structure pointing toward ring formation. Direct evidence of this ring formation can be observed from counting rings, from simulation snapshots, and from ring-size distributions shown in Figures 6, 9, and 10, respectively. The evolution of the total number of rings ( $N_{\text{ring}}$ ), shown in Figure 6, exhibits power-law relationships with the number of MC steps ( $N_{\text{MC}}$ ) of the form  $N_{\text{ring}} = k_i N_{\text{MC}}^{\gamma_i}$ , where  $k_i$  and  $\gamma_i$  are the power-law parameters of the *i*th stage. Figure 6 shows a sharp onset of ring formation at around 900 MC steps, with a power-law exponent of 2.5 in stage II. This stage exhibits the highest such power-law exponent, making this the ring-formation stage. This is the new stage that was not discussed by Devreux et al.<sup>8,9</sup>

Figure 10 shows that rings of size 4, 5, and 6 are mainly formed in this regime. As polymerization proceeds, larger ring sizes are also observed. Figure 9a shows a system snapshot at 2000 MC steps, with magnified pictures of a 4-ring (Figure 9b) and a 5-ring (Figure 9c). Figure 9a also shows the inhomogeneity of cluster size that exists during stage II.

The onset of ring formation once there is a substantial concentration of oligomers has two origins. In the first instance, the increase in the number and size of oligomers increases the probability of successful ring closing reaction moves. Second, the increase in the average particle size in the simulation lowers the cluster–cluster aggregation probability due to the effect of particle size on the diffusivities. In this regime, the polymerization is dominated by cross-linking condensation reactions. The increase in rate of ring formation with MC time is mainly due to the addition of small oligomers (monomers or dimers) to larger clusters. For example, when a monomer joins a large polymer, it can form four rings by cross-linking with other members of the same polymer, and every addition of such new monomer increases the possibility of ring formation. This analysis illustrates the impact of diffusion limitations that promote ring formation.



**Figure 11.** Variation of the radius of gyration for the silica clusters obtained from the MC simulations. The increase in  $R_g$  during 3300–6300 occurs due to cluster aggregation.



**Figure 12.** (a) The silica cluster containing 1000 monomeric units at the end of 0.1 million MC steps. The degree of condensation is  $c = 0.76$ . The brown, blue, and gray spheres indicate silicon, bridging oxygen, and hydroxyl groups, respectively. Subfigure b is a magnified view illustrating the local structure forming highly connected networks and rings.

We note that ring formation occurs in medium-sized clusters, e.g., rings of size 3–6, form in clusters of average size 20. The ring-formation stage is a significant feature of our predicted mechanism that is underemphasized in the literature,<sup>8,12–14</sup> likely because of the difficulty in measuring the presence of rings in silica.<sup>48</sup> During the ring-formation regime, the degree of condensation increases from 0.43 to 0.53, which based on our earlier comparison with experiment corresponds to an experimental time range between about 1 and 2.6 h.

**2.1.3. Cluster–Cluster Aggregation (3300–6300 MC Steps) and Gel Aging (6300–End).** After ring formation proceeds to a large extent, further cross-linking within clusters is not favored because of large energetic penalties for distorting network structures. In addition, the concentration of small oligomers in the system has decreased drastically, which also reduces the probability of small-oligomer assisted ring formation. As a result, the rate of ring formation falls at around 3300 MC steps, evidenced by the drop in the ring-formation power-law exponent: from 2.5 in stage II to only 1.5 in the present stage III (Figure 6). From the evolution of the average and maximum cluster sizes in Figure 7 and from the cluster-size distribution in Table 2, we see that by 6300 MC steps the cluster size has reached 1000, the initial number of monomers in the system and hence the maximum possible cluster size. The regime of 3300–6600 MC steps thus represents the next stage of polymerization.

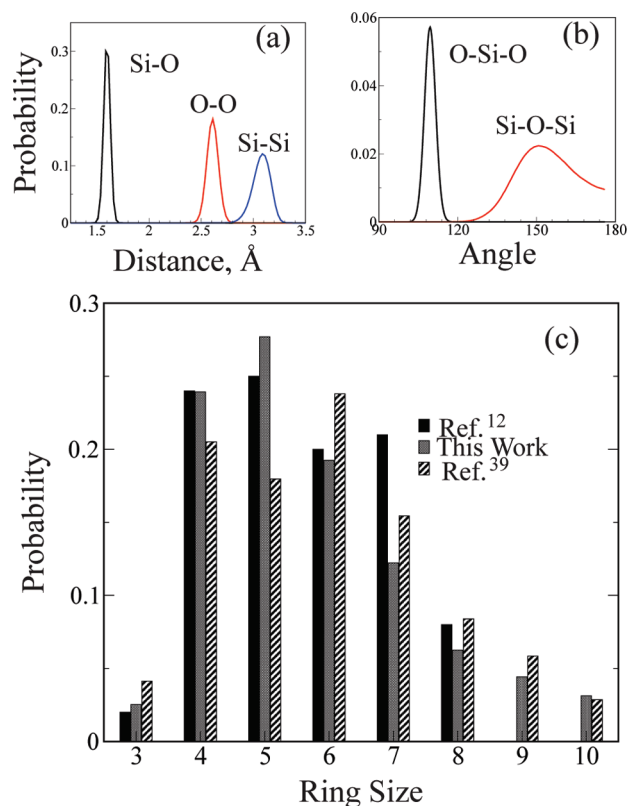


**Figure 13.** Probability of various bond lengths (a), bond angles (b), and ring-size distribution (c) obtained from our simulations. For comparison, the ring-size distributions obtained from previous studies of MD<sup>12</sup> and MC<sup>39</sup> simulations are also shown.

During this period, we see a rapid increase in the radius of gyration of the clusters, as shown in Figure 11. Beyond 6300 MC steps, we observe that the radius of gyration decreases very slowly due to aging of the silica gel. The value of the highest radius of gyration observed ( $\sim 42$  Å for 1000  $\text{Si}(\text{OH})_4$  system at 6300 MC steps) is due to the finite size of our simulation, and will in general depend on system size. However, the physics of this rapid increase is consistent for all (sufficiently large) system sizes. Taken together, the change in power-law behavior of ring formation and the rapid increase of both cluster size and radius of gyration point to cluster–cluster aggregation as the dominant mechanism in stage III. We note the distinction between this cluster–cluster aggregation involving large clusters and the aggregation in the oligomerization regime, which involves only monomers and small clusters. During stage III, the degree of condensation reaches the value  $c = 0.61$  which corresponds to about 5.6 h in the experiments. Our prediction of 5.6 h as the end of the cluster–cluster aggregation stage may depend on simulation system size. Figure 2 shows that the end of stage III, at 6300 MC steps, is the first point of discrepancy between experimental and simulated  $Q_n$  distributions, near the  $Q_2/Q_3$  crossing point.

Even after cluster aggregation, the mole fractions of  $Q_3$  and  $Q_4$  are significantly smaller than their final values. The value of the degree of condensation ( $c = 0.61$ ) indicates that polymerization is still not near completion, yet the cluster size has reached its maximum possible value given the system size. Further reaction requires cross-linking within the cluster (now a “gel”), which is slow because it always involves distortion of the network

**Table 3. Structural Parameters of Polymerized Silica**

	Si–O (Å)	O–O (Å)	Si–Si (Å)	O–Si–O (deg)	Si–O–Si (deg)
this work	1.58- (0.07)	2.61- (0.14)	3.09- (0.18)	109.5(5)	150.8(15)
MD <sup>49</sup>	1.62- (0.05)	2.64- (0.15)	3.10- (0.2)	109.6(10)	142(25)
MD <sup>52</sup>	1.6	2.52	3.2	108.1	159.3
Expt. <sup>53</sup>	1.62	2.65	3.12	109.5	144
Expt. <sup>54</sup>	1.62			109.4	153

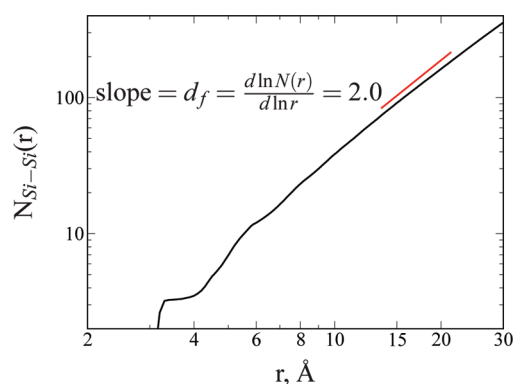
structure. This is the final stage denoted in the gel aging process, which has been documented in experiments.<sup>8</sup> During gel aging, as the cross-linking (or ring formation) continues, the availability of  $Q_1$  and  $Q_2$  decreases sharply. This decrease in concentration of reactant further requires large distortions of the gel, causing the rate of cross-linking to plummet in stage IV. This is consistent with ring formation in stage IV, where the power-law exponent falls below 1 to 0.6. This also helps to explain why silica condensation can take as long as 200 h under ambient, isoelectric conditions.<sup>8,9</sup>

**2.2. Structural Analysis.** Figure 12 shows a snapshot of a silica cluster containing 1000 monomeric units obtained after 0.1 million MC steps where the degree of condensation is 0.76. The resulting structure can be characterized by distributions of bond lengths, bond angles, and ring sizes. Figure 13a shows distributions of various bond lengths obtained during our simulations. The mean Si–O bond length extracted from Figure 13a is 1.59 Å with a full width at half-maximum of 0.07 Å. In general, zeolites<sup>3</sup> and different polymorphs of silica<sup>49</sup> exhibit Si–O bond lengths in the range 1.59–1.64 Å. The bond lengths obtained from our simulations thus compare well with other simulation and experimental studies as tabulated in Table 3. Distributions over O–Si–O and Si–O–Si angles are shown in Figure 13b and in Table 3; these also show very good agreement with previous experiments and simulations. The final ring-size distribution is shown in Figure 13c, where it is compared with results obtained from MD<sup>12</sup> and MC<sup>39</sup> simulations of other models. The detailed differences among these distributions reflect differences in the densities and temperatures studied, and in the underlying model assumptions. One characteristic of silica gel is the presence of three-membered rings, observed in all the simulation studies including ours (Figure 13c). In general, Figure 13c shows very good overall agreement between our final ring-size distributions and those from forcefield-based simulations.

We also investigate the fractal dimension from our simulations as a structural probe of the polymerized silica. The fractal dimension of a porous material can be obtained experimentally from small-angle X-ray scattering<sup>6,9</sup> or NMR.<sup>8</sup> The fractal dimension is a measure of how compact the silica clusters are. Experiments on silica gel obtained using sol–gel condensation processes at dilute concentrations (similar to the current study) have reported values in the range 2.0–2.3.<sup>6,9</sup> From our simulations, the fractal dimension is obtained using the following equation:<sup>50</sup>

$$d_f = \frac{d \ln N(r)}{d \ln r} \quad (8)$$

where  $N(r)$  is the number of atoms surrounding the central atom at a distance  $r$ .  $N(r)$  is obtained by integrating the radial distribution

**Figure 14.** Fractal dimension calculated from the slope of  $N_{\text{Si-Si}}(r)$  vs log–log plot.

function,  $g(r)$ . Considering that the fractal dimension is a long-range property, eq 8 applies at larger length scales. Figure 14 shows the log–log plot of  $N(r)$  obtained from our simulations, and the fractal dimension calculated from the slope is  $d_f = 2.0 \pm 0.1$ . This value compares very well with previous experimental<sup>6,9</sup> and simulation<sup>14</sup> results. Previous work<sup>6</sup> for silica gels obtained using sol–gel condensation suggests that the low fractal dimension (less than 3) arises from the cluster–cluster aggregation process, which leaves open spaces between aggregated clusters that do not close because of the sluggish process of gel relaxation. The results for our model are thus consistent with a very broad range of structural parameters for silica, from Si–O bond lengths all the way to the fractal dimension.

### 3. SUMMARY AND CONCLUSIONS

We have presented a new model and method for studying polymerization of silica by Monte Carlo (MC) simulation. The model focuses on flexible corner-sharing tetrahedra as the basic building block of polymerized silica. The condensation and hydrolysis reactions that determine the assembly process are simulated using the reaction ensemble MC (REMC) method, obviating the need for reactive force fields at the price of losing kinetic information on individual reactive events. The combination of a tetrahedron-based model and the REMC method allows an efficient study of the polymerizing silica system both at ambient temperatures and at low silicic acid concentrations typical of NMR characterization experiments. We find very good agreement with experiment for the evolution of the  $Q_n$  distribution with both time and degree of condensation, indicating that important aspects of the reaction mechanism are accurately captured by our simulations. Moreover, our simulations correctly capture the departures from the random branching model seen in the NMR experiments.

Our results suggest that polymerization starts with oligomerization followed by ring formation in the small oligomer units. These small oligomers with rings act as primary building units and aggregate to form larger clusters. Further reaction between the large clusters leads to gelation and aging. The mechanism is explained using cluster-size and ring-size distribution analysis. The resulting structure of silica reaches a high degree of condensation value of 0.76, and is characterized using fractal dimension and distributions over bond lengths, bond angles, and ring sizes. These structural parameters are in very good agreement with experiment, suggesting that our simulations have captured

atomic details as well as long-range structural aspects of silica polymerization. Our simulations point to a new regime in silica polymerization at intermediate times: ring formation. We have also found that the four stages of silica polymerization can be characterized by changes in the rates of ring formation. Our results thus point to the importance of characterizing rings in silica, which poses a significant challenge to experimental characterization methods. We emphasize that the observed polymerization mechanism corresponds to the isoelectric point at pH 2.5 and it will be interesting in future work to study the mechanism under other conditions.

In order to implement the REMC method, it was necessary to introduce some approximations. The first is the assumption of a constant standard Gibbs free energy across all condensation/hydrolysis reactions. Without this, the REMC method would be very challenging to apply in this context. There is support for this approximation from DFT calculations of the energetics of silica oligomers.<sup>43,44</sup> An additional approximation is the implementation of the force-bias method for increasing the likelihood of condensation reactions within silica polymers. It was not possible to correct for this bias, which may contribute to the relatively rapid onset of  $Q_3$  and  $Q_4$  relative to experiment. A third approximation concerns the treatment of cluster diffusion when considering cluster-cluster aggregation moves, which may also contribute to the rapid onset of higher-order structures in the simulations. In addition to these approximations, we have used fixed probabilities for various moves, which represent different time scales (such as bond vibrations (BO/HG vertex moves) vs cluster translation moves), and the evolution of  $Q_n$  distribution may have some sensitivity to variations in the relative attempt probabilities. These approximations were necessary to enable the REMC simulations to generate substantial polymerization under ambient conditions. While we recognize the ad hoc quality of these assumptions, we are somewhat reassured by the quality of the agreement with experiment on the kinetics of the  $Q_n$  distribution, and on the structural aspects of the resulting silica gel. Developing more rigorous alternatives to these approximations, as well as finding how the distribution of attempt frequencies among the types of MC moves might relate to real processing conditions, remains a priority for future work.

Given the apparent utility of our new model in studying silica polymerization and the relative efficiency with which it can be implemented, we believe it offers new opportunities for studying silica polymerization in other circumstances such as the growth of zeolites or the formation of ordered mesoporous silica materials. We plan to explore these in future work.

## APPENDIX

**A. Implementation of Condensation Move.** To implement the condensation move, we have used the idea of a reaction cutoff. This is well known in the simulation field and has been implemented for network polymerization.<sup>51</sup> In the reaction cutoff method, particles within the cutoff are given a high probability for reaction as compared to particles that are far away. The method introduces bias by selecting a particle from a subset of the total available reactant. This bias can be corrected easily by weighting the transition probability during the acceptance of the move. In general, for a selected pair of hydroxyl groups,  $\text{OH}^{(1)}$  and  $\text{OH}^{(2)}$ , the condensation reactions would be either (a) cluster aggregation (where  $\text{OH}^{(1)}$  and  $\text{OH}^{(2)}$  are part of different clusters); (b) cross-linking within the reaction cut-off ( $r\text{OH1} - r\text{OH2} < R_c$ ) or

(c) cross-linking outside the reaction cut-off ( $r\text{OH1} - r\text{OH2} > R_c$ ). On the basis of these situations, we employ the following scheme while carrying out condensation reactions:

- From the system containing  $N_{\text{OH}}$  number of hydroxyl groups (OH), select one OH randomly,  $\text{OH}^{(1)}$ .
- Identify the cluster of  $\text{OH}^{(1)}$  and find the size of the cluster ( $N_{\text{cl1}}$ ) and the total number of OHs ( $N_{\text{OH,cl1}}$ ) present on the cluster.
- On the basis of  $N_{\text{cl1}}$ , find the probability of cluster aggregation ( $p_1$ ), cross-linking within the reaction cutoff ( $p_2$ ), and cross-linking outside the reaction cutoff ( $p_3$ ). The numerical values of these different probabilities were defined on the basis of the following heuristic approach. (a) For a given cluster of size  $N_{\text{cl}}$ , the probability to react with another cluster/monomer depends on its diffusivity. Hence,  $p_1 \propto D_{\text{cl}} \propto 1/N_{\text{cl}}$ . For large  $N_{\text{cl}}$ , the numerical value becomes extremely small; hence, we used  $p_1 = 1/N_{\text{cl}}$  for  $N_{\text{cl}} < 30$  and  $p_1 = 1/30$  for  $N_{\text{cl}} \geq 30$ . (b) In cross-linking, for a given reactant  $i$  in a cluster  $N_{\text{cl}}$ , the number of collisions with other particles in proximity will always be constant due to strong repulsive short-range interactions. Hence, its diffusivity in the proximity region would also be constant and independent of cluster size. On the basis of this, the probability of cross-linking within the reaction cutoff is chosen to be  $p_2 = 0.2$  for  $N_{\text{cl}} > 2$ . Experimentally, cross-linking in dimers (two-membered ring) is not observed at room temperature and hence excluded in our definition as well. (c) The probability of cross-linking outside the reaction cutoff is  $p_3 = 1 - p_2 - p_1$ .
- After estimating  $p_1$ ,  $p_2$ , and  $p_3$  based on  $N_{\text{cl1}}$ , generate a random number  $\xi$ .
- If  $\xi < p_1$ , cluster aggregation:
  - Select a second hydroxyl group,  $\text{OH}^{(2)}$ , which does not belong to the  $N_{\text{cl1}}$  cluster.
  - Translate the selected cluster such that  $|\mathbf{r}_{\text{OH1}} - \mathbf{r}_{\text{OH2}}| = 0$ .
  - Reject move if hard sphere overlaps are present.
  - Replace  $\text{OH}^{(1)}$  and  $\text{OH}^{(2)}$  with a bridging oxygen and calculate the change in energy.
  - Accept the reaction with a corrected probability

$$P_{\text{rxn}}^{\text{corr}} = \frac{1}{p_1} \frac{(N_{\text{OH}} - N_{\text{OH,cl1}})}{N_{\text{OH}} - 1} \frac{1}{N_{\text{MC},ij}} P_{\text{rxn}} \quad (9)$$

where

$$P_{\text{rxn}} = e^{-\beta\Delta U} \frac{(N_w + 1)(N_{\text{BO}} + 1)}{(N_{\text{OH}} - 2)(N_{\text{OH}} - 1)} K_{\text{eq}} \quad (10)$$

$\Delta U$  is the change in potential energy,  $K_{\text{eq}}$  is the equilibrium constant, and  $N_w$  and  $N_{\text{BO}}$  are the number of water molecules and bridging oxygens present in the system, respectively. In eq 9, the first term is the correction for cluster-aggregation probability, the second term is a correction for selecting OH from a smaller subset, and the third term corrects for the translation of clusters toward each other. This ensures that the reaction probability of the overall move is free from bias.

- If  $p_1 < \xi < p_1 + p_2$ , cross-linking within the reaction cutoff:
  - Identify all hydroxyl groups that are part of the same cluster and within the reaction cutoff of  $\text{OH}^{(1)}$ ,  $N_{\text{OH,wc}}$ .
  - Select  $\text{OH}^{(2)}$  randomly from this subset.
  - Replace  $\text{OH}^{(1)}$  and  $\text{OH}^{(2)}$  with a bridging oxygen.

- Perform force–bias MC moves if required. Note that the bias introduced during force–bias cannot be removed and hence a small number of such moves are employed.
- Accept the reaction with a corrected probability

$$p_{\text{rxn}}^{\text{corr}} = \frac{1}{p_2} \frac{N_{\text{OH},\text{wc}}}{N_{\text{OH}} - 1} p_{\text{rxn}} \quad (11)$$

where the first term is the correction for cross-linking within the reaction cutoff and the second term is a correction for selecting OH from a smaller subset.

- If  $p_1 + p_2 < \xi < 1$ , cross-linking outside the reaction cutoff:
  - Identify all hydroxyl groups that are part of the same cluster and outside the reaction cutoff of  $\text{OH}^{(1)}$ ,  $N_{\text{OH},\text{oc}}$ .
  - Select  $\text{OH}^{(2)}$  randomly from this subset.
  - Replace  $\text{OH}^{(1)}$  and  $\text{OH}^{(2)}$  with a bridging oxygen.
  - Perform force–bias MC moves if required.
  - Accept the reaction with a corrected probability

$$p_{\text{rxn}}^{\text{corr}} = \frac{1}{p_3} \frac{N_{\text{OH},\text{oc}}}{N_{\text{OH}} - 1} p_{\text{rxn}} \quad (12)$$

where the first term is the correction for cross-linking outside the reaction cutoff probability and the second term is a correction for selecting OH from a smaller subset.

We have performed sensitivity analysis of the results on the reaction cutoff by obtaining results for  $R_c = 3$  and  $6 \text{ \AA}$ . Since the biases introduced due to reaction cutoff are corrected during acceptance of moves, the  $Q_n$  distribution does not change appreciably by changing the reaction cutoff.

**B. Force–Bias Moves.** Condensation reactions within a given cluster lead to ring formation. However, due to high strain energy, the sampling of this event is very poor during simulations. An alternative is to perform the condensation reaction and regrow the entire cluster. However, currently there is no method available that can regrow a complex, three-dimensional network cluster maintaining detailed balance. Hence, another advanced technique needs to be employed in order to overcome the poor sampling of ring formation. Here, we use the force–bias method. We emphasize that the bias introduced due to the force–bias method is not removed completely, but it can be mitigated by employing small numbers of such moves. The protocol employed for force–bias methods is as follows:

- Select and calculate the forces on atom  $i$  (vertex of a tetrahedron, OH/BO) of a given cluster.
- Attempt the atom (vertex) displacement move. The atoms are displaced in the direction of force to relax the system, i.e.,  $\Delta \mathbf{r}_i = \mathbf{e}_i \cdot \Delta r_{\text{max}}$  where  $\Delta r_{\text{max}}$  is the maximum displacement within which an atom can be moved and  $\Delta \mathbf{r}_i$  and  $\mathbf{e}_i$  are the displacement vector and unit vector of force on atom  $i$ , respectively.
- If a move is accepted, update the energy,  $U_i$ , and configuration of the system,  $\mathbf{X}_i$ , or else retain the previous configurations and energy.
- Repeat the above steps for all vertices of the selected cluster. Force–bias moves are performed on all particles of the selected cluster only, and the rest of the system is kept fixed. In these simulations, we have executed 500 such force–bias MC moves for each attempted intracuster condensation event.

## AUTHOR INFORMATION

### Corresponding Author

\*E-mail: auerbach@chem.umass.edu (S.M.A.); monson@ecs.umass.edu (P.A.M.).

## ACKNOWLEDGMENT

This work was supported by a grant from the U.S. Department of Energy (Contract No. DE-FG02-07ER46466). A.M. thanks Forum Thakkar for useful discussions.

## REFERENCES

- (1) Iler, R. K. *The Chemistry of Silica*; Wiley: New York, 1979.
- (2) Brinker, C. J.; Scherer, G. W. *Sol-gel science*; Academic Press: San Diego, CA, 1990.
- (3) Auerbach, S. M., Carrado, K. A., Dutta, P. K., Eds. *Handbook of Zeolite Science and Technology*; Marcel Dekker Inc.: New York, 2003.
- (4) Beck, J.; Vartuli, J.; Roth, W.; Leonowicz, M. *J. Am. Chem. Soc.* **1992**, *114*, 10834–10843.
- (5) Kresge, C. T.; Leonowicz, M. E.; Roth, W. J.; Vartuli, J. C.; Beck, J. S. *Nature* **1992**, *359*, 710–712.
- (6) Schaefer, D. W.; Keefer, K. D. *Phys. Rev. Lett.* **1986**, *56*, 2199–2202.
- (7) Vega, A. J.; Scherer, G. W. *J. Non-Cryst. Solids* **1989**, *111*, 153–166.
- (8) Devreux, F.; Boilot, J. P.; Chaput, F.; Lecomte, A. *Phys. Rev. A* **1990**, *41*, 6901–6909.
- (9) Devreux, F.; Boilot, J. P.; Chaput, F.; Sapoval, B. *Phys. Rev. Lett.* **1990**, *65*, 614–617.
- (10) Brunet, F.; Cabane, B.; Dubois, M.; Perly, B. *J. Phys. Chem.* **1991**, *95*, 945–951.
- (11) Feuston, B. P.; Garofalini, S. H. *J. Phys. Chem.* **1990**, *94*, 5351–5356.
- (12) Garofalini, S. H.; Martin, G. J. *J. Phys. Chem.* **1994**, *98*, 1311–1316.
- (13) Rao, N. Z.; Gelb, L. D. *J. Phys. Chem. B* **2004**, *108*, 12418–12428.
- (14) Bhattacharya, S.; Kieffer, J. *J. Chem. Phys.* **2005**, *122*, 094715.
- (15) Bhattacharya, S.; Kieffer, J. *J. Phys. Chem. C* **2008**, *112*, 1764–1771.
- (16) Auerbach, S. M.; Ford, M. H.; Monson, P. A. *Curr. Opin. Colloid Interface Sci.* **2005**, *10*, 220–225.
- (17) Astala, R.; Auerbach, S. M.; Monson, P. A. *J. Phys. Chem. B* **2004**, *108*, 9208–9215.
- (18) Astala, R.; Auerbach, S. M.; Monson, P. A. *Phys. Rev. B* **2005**, *71*, 014112.
- (19) Flanigen, E.; Bennett, J.; Grose, R.; Cohen, J.; Patton, R.; Kirchner, R.; Smith, J. *Nature* **1978**, *271*, 512–516.
- (20) Zhao, D.; Feng, J.; Huo, Q.; Melosh, N.; Fredrickson, G.; Chmelka, B.; Stucky, G. *Science* **1998**, *279*, 548–552.
- (21) Pouxviel, J. C.; Boilot, J. P. *J. Non-Cryst. Solids* **1987**, *94*, 374–386.
- (22) Kay, B. D.; Assink, R. A. *J. Non-Cryst. Solids* **1988**, *104*, 112–122.
- (23) Bailey, J. K.; Macosko, C. W.; McCartney, M. L. *J. Non-Cryst. Solids* **1990**, *125*, 208–223.
- (24) Assink, R. A.; Kay, B. D. *Annu. Rev. Mater. Sci.* **1991**, *21*, 491–513.
- (25) Assink, R. A.; Kay, B. D. *J. Non-Cryst. Solids* **1988**, *107*, 35–40.
- (26) Kasehagen, L. J.; Rankin, S. E.; McCormick, A. V.; Macosko, C. W. *Macromolecules* **1997**, *30*, 3921–3929.
- (27) Rankin, S. E.; Kasehagen, L. J.; McCormick, A. V.; Macosko, C. W. *Macromolecules* **2000**, *33*, 7639–7648.
- (28) Sefcik, J.; Rankin, S. E. *J. Phys. Chem. B* **2003**, *107*, 52–60.
- (29) Jorge, M.; Auerbach, S. M.; Monson, P. A. *J. Am. Chem. Soc.* **2005**, *127*, 14388–14400.

- (30) Schumacher, C.; Gonzalez, J.; Wright, P. A.; Seaton, N. A. *J. Phys. Chem. B* **2006**, *110*, 319–333.
- (31) Jorge, M.; Gomes, J. R. B.; Natalia, M.; Cordeiro, D. S.; Seaton, N. A. *J. Phys. Chem. B* **2009**, *113*, 708–718.
- (32) Petrovich, R. *Geochim. Cosmochim. Acta* **1981**, *45*, 1665–1674.
- (33) Tester, J.; Worley, W.; Robinson, B.; Grigsby, C.; Feerer, J. *Geochim. Cosmochim. Acta* **1994**, *58*, 2407–2420.
- (34) Dove, P. M.; Han, N.; Wallace, A. F.; De Yoreo, J. J. *Proc. Natl. Acad. Sci. U.S.A.* **2008**, *105*, 9903–9908.
- (35) Lasaga, A.; Gibbs, G. *Am. J. Sci.* **1990**, *290*, 263–295.
- (36) Bandstra, J. Z.; Brantley, S. L. *Geochim. Cosmochim. Acta* **2008**, *72*, 2587–2600.
- (37) Nangia, S.; Garrison, B. J. *J. Am. Chem. Soc.* **2009**, *131*, 9538–9546.
- (38) Malani, A.; Auerbach, S. M.; Monson, P. A. *J. Phys. Chem. Lett.* **2010**, *1*, 3219–3224.
- (39) Wu, M. G.; Deem, M. W. *J. Chem. Phys.* **2002**, *116*, 2125.
- (40) Astala, R.; Auerbach, S. M. *J. Am. Chem. Soc.* **2004**, *126*, 1843–1848.
- (41) Smith, W. R.; Triska, B. *J. Chem. Phys.* **1994**, *100*, 3019.
- (42) Johnson, J. K.; Panagiotopoulos, A. Z.; Gubbins, K. E. *Mol. Phys.* **1994**, *81*, 717–733.
- (43) Pereira, J. C. G.; Catlow, C. R. A.; Price, G. D. *J. Phys. Chem. A* **1999**, *103*, 3268–3284.
- (44) Nangia, S.; Garrison, B. J. *Mol. Phys.* **2009**, *107*, 831–843.
- (45) Catlow, C. R. A.; Ackermann, L.; Bell, R. G.; Cora, F.; Gay, D. H.; Nygren, M. A.; Pereira, J. C.; Sastre, G.; Slater, B.; Sinclair, P. E. *Faraday Discuss.* **1997**, *106*, 1–40.
- (46) Yuan, X.; Cormack, A. N. *Comput. Mater. Sci.* **2002**, *24*, 343–360.
- (47) Sevick, E. M.; Monson, P. A.; Ottino, J. M. *J. Chem. Phys.* **1988**, *88*, 1198–1206.
- (48) Kohara, S.; Suzuya, K. *J. Phys.: Condens. Matter* **2005**, *17*, S77–S86.
- (49) Vashishta, P.; Kalia, R. K.; Rino, J. P.; Ebbsjo, I. *Phys. Rev. B* **1990**, *41*, 12197.
- (50) Kieffer, J.; Angell, C. A. *J. Non-Cryst. Solids* **1988**, *106*, 336–342.
- (51) Galina, H.; Lecowicz, J. B. *Macromol. Symp.* **2001**, *171*, 37–44.
- (52) Kubicki, J. D.; Lasaga, A. C. *Am. Mineral.* **1988**, *73*, 941–955.
- (53) Mozzi, R. L.; Warren, B. E. *J. Appl. Crystallogr.* **1969**, *2*, 164–172.
- (54) DaSilva, J. R. G.; Pinatti, D. G.; Anderson, C. E.; Rudee, M. L. *Philos. Mag. A* **1975**, *31*, 713–717.